Quantum Mechanical Study on the Facial Selectivity of Dioxa and Trioxa Cage Molecules

Ito Chao,*,† J. H. Shih,† and Hsien-Jen Wu*,‡

Institute of Chemistry, Academia Sinica, Nankang, Taipei, Taiwan, and Department of Applied Chemistry, Chiao Tung University, Hsinchu, Taiwan

ichao@chem.sinica.edu.tw

Received June 7, 2000

High facial selectivity (>99%) of nucleophilic addition to the carbonyl groups of the title compounds (**1** and **2**) has been achieved for the novel trioxa cage **2**, but not for the dioxa **1**. Similar experimental observations were made for the carbene addition to the double bonds of cage compounds, **3** and **4**. Calculations were carried out for the cage compounds and their reaction transition structures, with LiH as a nucleophile and $:CCl_2$ as an attacking carbene. The calculated facial preference for nucleophilic and carbene addition agreed well with experimental results. The origins of facial selectivity are examined from the viewpoints of structure, frontier orbitals, and molecular electrostatic potential of the reactants, as well as strain, electrostatic, and hyperconjugation effects in the transition state. For dioxa cages, the structural facial difference around the reaction center is minor, but the electronic difference of syn and anti faces generated by the two remote oxygen atoms is clearly demonstrated via frontier orbital and MEP analyses. For trioxa cages, the close proximity of the third ether oxygen (O_s) to the reaction center brings large structural and electronic changes around the reaction center. The calculated electrostatic and strain energy differences of syn and anti transition structures are significantly larger for trioxa cages than for the dioxa cages. Therefore, they both contribute to the enhanced facial selectivity of trioxa compounds. Finally, analysis of hyperconjugative stabilization in transition structures reveals the danger of relying solely on Cieplak or Anh models in rationalization of facial selectivity, especially when nonequivalent steric and electrostatic effects as those present in the trioxa systems are involved.

Introduction

Since the first rule proposed by Cram[1] in 1952 to explain the diastereofacial selectivity in the addition of nucleophiles to α-chiral carbonyl compounds, organic chemists have not ceased to construct models that provide rationalizations and predictions for preferential addition to one π-face over the other of a trigonal carbon center. In Cram's rule, the largest group attached to the α-carbon should be anti to the carbonyl group and the nucleophile approaches the carbonyl group from the side with less steric congestion. Similar to Cram's rule, the Felkin−Anh model[2,3] also considers the conformation of substituents of the α-carbon and the steric effect encountered by an incoming nucleophile. However, in this model the largest group is perpendicular to the plane of the carbonyl group and is antiperiplanar to the nucleophile. In addition, Anh and Eisenstein stressed the importance of electronic effect in the transition state. They suggested a heteroatom such as Cl should be placed antiperiplanar to the nucleophile since the low lying σ_{C-X}* could lower the π_{CO}* and stabilized the transition state.[3,4] Another way of putting it, the transition state can be stabilized by the hyperconjugation between the incipient bond, which involves the nucleophile and the π_{CO}*, and the vacant antiperiplanar antibonding orbital of a vicinal sigma bond. For cyclic ketones, where the conformation around the α-carbon is relatively rigid comparing to acyclic ketones, the Felkin model also identified the so-called "torsional strain"[2] factor. This factor has been used as one of the reasons why nonbulky hydrides attack unhindered cyclohexanones from the axial side rather than the equatorial. In the axial approach the incipient bond may suffer from 1,3 diaxial-type interactions, but this forming bond in the transition structure is basically staggered with groups attached to the α-carbon. On the other hand, in the equatorial approach the incipient bond is nearly eclipsed to the vicinal bonds and hence this approach is unfavorable in terms of torsional strain. Houk et al. developed an empirical force field (modified MM2) to model transition states of nucleophilic additions to carbonyls.[5] The calculated product ratios were in excellent agreement with experiment for acyclic and cyclic ketones and provided strong support to the Felkin model.

In the early 1980s, Cieplak provided another model which is also of electronic origin.[6] Contrary to the hyperconjugation in the Felkin−Anh model between the

* To whom correspondence should be addressed. Phone: ++886-2-2789-8530. Fax: ++886-2-2783-1237.

† Academia Sinica.

‡ Chiao Tung University.

(1) (a) Cram, D. J.; Elhafez, F. A. A. *J. Am. Chem. Soc.* **1952**, *74*, 5828. (b) Mengel, A.; Reiser, O. *Chem. Rev.* **1999**, *99*, 1191.

(2) Chérest, M.; Felkin, H.; Prudent, N. *Tetrahedron Lett.* **1968**, *18*, 2199.

(3) (a) Anh, N. T. *Top. Curr. Chem.* **1980**, *88*, 145. (b) Anh, N. T.; Eisenstein, O. *Nouv, J. Chim.* **1977**, *1*, 61. (c) Anh, N. T.; Eisenstein, O. *Tetrahedron Lett.* **1976**, *3*, 155.

(4) Anh, N. T.; Eisenstein, O.; Lefour, J.-M.; Tran Huu Dau, M. E. *J. Am. Chem. Soc.* **1973**, *95*, 6146.

(5) (a) Wu, Y.-D.; Houk, K. N. *J. Am. Chem. Soc.* **1987**, *109*, 908. (b) Wu, Y.-D.; Houk, K. N.; Trost, B. M. *J. Am. Chem. Soc.* **1987**, *109*, 5560.

(6) (a) Cieplak, A. S. *J. Am. Chem. Soc.* **1981**, *103*, 4540. (b) Cieplak, A. S.; Tait, B. D.; Johnson, C. R. *J. Am. Chem. Soc.* **1989**, *111*, 8447.

10.1021/jo000872j CCC: $19.00
Published on Web 09/29/2000

incipient bond and the vacant antibonding orbital of an antiperiplanar vicinal bond, Cieplak emphasized the importance of hyperconjugation between the filled orbital of a vicinal bond and the antibonding orbital of the incipient bond. In brief, the Cieplak model predicts that the addition reaction takes place on the face that is anti to the electron rich vicinal bonds. This model has been applied successfully to nucleophilic addition to carbonyl compounds, electrophilic addition to olefins, cycloadditions and many other reactions.[7] Nevertheless, just as other aforementioned models, the Cieplak model does not always lead to correct predictions and has been challenged on the basis of theoretical and experimental results.[8] One of the effects that are often invoked to provide an alternative explanation to the Cieplak-type hyperconjugation is the electrostatic effect.[9,10] Computationally, this effect has been estimated by placing point charges next to the reaction center of a ground-state reactant[11] or a reaction transition structure with removal of the nuclephile.[10] Experimentally, a good correlation between logarithm of the product ratio and electrostatic field parameters (σ_F) has been taken as an indication for the presence of electrostatic effect.[12]

Analyses based on ground-state reactant properties have also been shown useful in predicting π-facial selectivity. Gung and others studied the structure distortion of reactants such as heteroatom-substituted cyclohexanones and admantanones.[13] Mehta et al. illustrated that the facial molecular electrostatic potential of methylenenorsnoutanes was affected by remote substitution.[14] Klein,[15] Fukui,[16] Frenking,[17] and Ohwada[18] pointed out the unequal facial distribution of frontier orbitals. Liotta,[19] Dannenberg,[20] and Tomoda[21] developed methods attempting to quantify the orbital distortion, unequal facial electron distribution, or accessible space. Adcock measured the NMR chemical shifts of reactants or their analogues to shed light on the origin of facial selectivity.[22] Overall, there are many different opinions and debates on the issue of origins of facial selectivity.[8] Recently, one issue of Chemical Review was entirely devoted to models and physical organic investigations of diastereofacial selectivity and synthetic strategies for achieving selectivity.[23]

One of us has synthesized dioxa and novel trioxa cage compounds **1**−**4**. Ketones **1** and **2** were subjected to nucleophilic addition by $NaBH_4$ and CH_3MgBr and alkenes **3** and **4** were treated with dichlorocarbene. For dioxa cages (**1** and **3**), the addition reactions took place on both sides of the trigonal carbons, with a preference at the face syn to the oxygen atoms in the cage. For trioxa compounds (**2** and **4**), additions took place essentially at the face anti to the oxygen atoms (product ratio >99: <1).[24] Hydride ($NaBH_4$) reduction of **1** has been reported

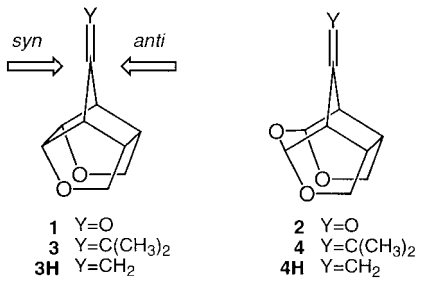

1 Y=O
3 Y=C(CH$_3$)$_2$
3H Y=CH$_2$

2 Y=O
4 Y=C(CH$_3$)$_2$
4H Y=CH$_2$

by Mehta et al.[25] They demonstrated the correlation between electrostatic effect and syn attack preference with charge replacement ab initio calculations[25a] and σ_F deduced from ^{13}C NMR chemical shift data.[25b] Other effects such as distortion of structure and frontier orbitals, torsional strain and hyperconjugation were not addressed. If electrostatic factor is important in the hydride reduction of dioxa cage **1**, which involves highly polar nucleophilic attacking species, is it also important for the addition reaction of dioxa cage **3** with a relative neutral electrophilic dichlorocarbene?[26] If hyperconjugation, be it of Cieplak-type or Anh-type, does play a role, does it help to achieve the excellent facial selectivity observed for addition reactions of trioxa cages **2** and **4**? Does the filled nonbonded lone pair orbital of the additional oxygen atom in **2** and **4** also interacts with the antibonding of the incipient bond? Conceivably, introduction of oxygen atoms in the cage should generate certain structure distortion around the reaction center. How does this distortion correlate with facial selectivity?

In this paper, we report theoretical studies of hydride reduction of **1** and **2** and carbene addition of **3** and **4**. It has been shown that calculations with LiH for ketone reduction reproduce the trends observed experimentally in $NaBH_4$ reduction.[8,27] Therefore, LiH was used in our calculations for hydride reduction for the sake of computational efficiency. In terms of carbene addition, dichlorocarbene, a singlet carbene in the ground state,[26,28] is used in calculations as in experiments. Nevertheless, the methyl groups on the terminal alkene carbon of **3** and **4** are replaced with hydrogens in calculations and labeled as **3H** and **4H**. The controversial Cieplak-type hyperconjugation, as well as the Anh-type, are evaluated by the Natural Bond Orbital (NBO) analysis of Weinhold et al.[29] The unsymmetrical facial distribution of frontier

(7) Kaselj, M.; Chung, W.-S.; le Noble, W. J. *Chem. Rev.* **1999**, *99*, 1387 and references therein.
(8) Gung, B. W. *Tetrahedron* **1996**, *52*, 5263.
(9) (a) Wong, S. S.; Paddon-Row, M. N. *J. Chem. Soc., Chem. Commun.* **1991**, 327. (b) Wong, S. S.; Paddon-Row, M. N. *Aust. J. Chem.* **1991**, *44*, 765. (c) Wu, Y -D.; Tucker, J. A.; Houk, K. N. *J. Am. Chem. Soc.* **1991**, *113*, 5018.
(10) Paddon-Row, M. N.; Wu, Y.-D.; Houk, K. N. *J. Am. Chem. Soc.* **1992**, *114*, 10638.
(11) Ganguly, B.; Chandrasekhar, J.; Khan, F. A.; Mehta, G. *J. Org. Chem.* **1993**, *58*, 1734.
(12) Adcock, W.; Cotton, J.; Trout, N. A. *J. Org. Chem.* **1994**, *59*, 1867.
(13) (a) Gung, B. W.; Wolf, M. A.; Mareska, D. A.; Karipides, A. *J. Org. Chem.* **1994**, *59*, 4899. (b) Gung, B. W. *Chem. Rev.* **1999**, *99*, 1377. (c) Gung, B. W.; Wolf, M. A. *J. Org. Chem.* **1996**, *61*, 232.
(14) Mehta, G.; Ravikrishna, C.; Gadre, S. R.; Suresh, C. H.; Kalyanaraman, P.; Chandrasekhar, J. *J. Chem. Soc., Chem. Commun.* **1998**, 975.
(15) Klein, J. *Tetrahedron Lett.* **1973**, 4307.
(16) Fukui, K. *Theory of Orientation and Stereoselection*; Springer-Verlag: Heidelberg, 1979.
(17) Frenking, G.; Kohler, K. F.; Reetz, M. T. *Angew. Chem., Int. Ed. Engl.* **1991**, *30*, 1146.
(18) Ohwada, T. *Chem. Rev.* **1999**, *99*, 1337 and references therein.
(19) (a) Liotta, C. L. *Tetrahedron Lett.* **1975**, 519. (b) Liotta, C. L.; Burgess, E. M.; Eberhardt, W. H. *J. Am. Chem. Soc.* **1984**, *106*, 4849.
(20) (a) Huang, X. L.; Dannenberg, J. J.; Duran, M.; Bertrán, J.*J. Am. Chem. Soc.* **1993**, *115*, 4024. (b) Huang, X. L.; Dannenberg, J. J. *J. Am. Chem. Soc.* **1993**, *115*, 6017.
(21) (a) Tomoda, S. *Chem. Rev.* **1999**, *99*, 1243 and references therein. (b) Tomoda, S.; Senju, T. *J. Chem. Soc., Chem. Commun.* **1999**, 621.
(22) Adcock, W.; Trout, N. A. *Chem. Rev.* **1999**, *99*, 1415 and references therein.
(23) Gung, B. W.; le Noble, B., Eds, *Chemical Reviews*, **1999**, *5*.
(24) Wu, H. J.; Wu. C. Y.; Lin, H. C.; Chao, C. S.; Chao, I.; Shih, J. H. Manuscript in preparation.
(25) (a) Mehta, G.; Khan, F. A.; Ganguly, B.; Chandrasekhar, J. *J. Chem. Soc., Perkin Trans. 2* **1994**, 2275. (b) Mehta, G.; Khan, F. A.; Adcock W. *J. Chem. Soc., Perkin Trans. 2* **1995**, 2189.
(26) Moss, R. A. *Acc. Chem. Res.* **1980**, *13*, 58.

orbitals or electrostatic potential are investigated qualitatively by mapping the values of the specific property onto the electron density isosurface of the reactant.[30,31]

Computational Methods

All geometry optimization calculations were performed with GAUSSIAN 94[32] or GAUSSIAN 98[33] program suites at the theory level of HF/6-31G*. This level has been shown to correctly predict facial selectivity of related systems.[10,25a] Each stationary point was characterized as a minima or a transition state by frequency calculations. All the transition states were further characterized by analysis of the vibrational modes corresponding to their imaginary frequencies. Frontier molecular orbitals (HOMO and LUMO) or molecular electrostatic potential (MEP) of a substrate were mapped onto its isosurface with electron density of 0.002 au with the Spartan 4.1.1 program.[34] Natural bond orbital (NBO) analysis and the second-order perturbative stabilization energy of transition states were carried out and evaluated with the program NBO 4.0.[35]

Results and Discussion

Activation Energies. The product ratio observed experimentally for $NaBH_4$ reduction of dioxa cage **1** is 85:15 (syn/anti) and of trioxa cage **2** is <1:>99; for dichlorocarbene addition of dioxa **3** is 60:40 and of trioxa **4** is <1:>99. In other words, the syn attack is favored for dioxa cages and the anti attack is favored for trioxa cages. The calculation results at HF/6-31G* level are listed in Table 1, and they correlate well with the observed facial selectivity. For example, the energy differences of syn and anti transition structures of dioxa cages **1** and **3H** are 1.26 and 0.43 kcal/mol, respectively, leading to higher activation energies for the anti attack and thus higher percentage of the syn product. For trioxa cages **2** and **4H**, the energy differences of syn and anti transition structures (more than 3.8 kcal/mol) are significantly higher than that of dioxa cages **1** and **3H**. Therefore, the effectively exclusive anti addition in the trioxa systems is successfully modeled by our calculations.

Table 1. Calculated Energies of Addition Transition Structures[a] with Full Geometry Optimization at the HF/6-31G* Level

	E (au)	ΔE^b (kcal/mol)
1-*syn*	−579.189 66	0.00
1-*anti*	−579.187 65	1.26
2-*syn*	−654.061 45	4.66
2-*anti*	−654.068 88	0.00
3H$_a$-*syn*	−1492.028 92	0.00
3H$_a$-*anti*	−1492.028 23	0.43
3H$_b$-*syn*	−1492.026 61	1.45
3H$_b$-*anti*	−1492.027 30	1.02
4H$_a$-*syn*	−1566.900 37	5.57
4H$_a$-*anti*	−1566.909 25	0.00
4H$_b$-*syn*	−1566.903 08	3.87
4H$_b$-*anti*	−1566.908 51	0.46

[a] Labels *syn* and *anti* represent the additions from the syn and anti faces, respectively. Transition states of LiH addition to ketones **1** and **2** and that of dichlorocarbene addition to enes **3H** and **4H** are calculated. Labels *a* and *b* represent the addition trajectories with the carbon lone pair of dichlorocarbene pointing to the inner ene carbon, C_t, and the outer one, Y, respectively. [b] Energies relative to the lowest transition structure are shown.

It is noted that in dichlorocarbene addition, four different transition structures were located. This is because the transition state is asynchronous in terms of the two forming bonds. We define the trajectory in which the bond with larger degree of formation involves the inner ene carbon as "trajectory ***a***" and that involves the terminal ene carbon as "trajectory ***b***". For **3H**, both syn and anti attacks favor trajectory ***a*** (see **3H**$_a$-***syn***, **3H**$_a$-***anti***, **3H**$_b$-***syn***, **3H**$_b$-***anti*** in Table 1; transition structures are shown in Figure 7). However, for **4H** trajectory ***a*** is lower in energy for the anti attack, but trajectory ***b*** is lower for the syn attack (transition structures are shown in Figure 8). We will discuss this change of preferred trajectory in more details in a later section.

On the basis of satisfactory predictions of facial selectivity by calculated energy differences of transition structures, results at the HF/6-31G* level are used for further analyses.

Structures and Properties of Dioxa and Trioxa Cages. Calculated structures and atom labels of the cage compounds are shown in Figure 1. The effect of the two oxygen atoms on structural distortion of the dioxa cages is rather minor. It is shown in Table 2 that hydrogens (H_{b1} and H_{b2}) on the bridgehead carbons (C_{b1} and C_{b2}) twist out of the carbonyl plane by less than 1° (see dihedral angles $Y-C_t-C_{b1}-H_{b1}$ and $Y-C_t-C_{b2}-H_{b2}$ in Table 2); for **1** the bridgehead hydrogens lean toward the syn side and for **3H** toward the anti side. The difference between dihedral angles $Y-C_t-C_{b1}-C_{s1}$ and $Y-C_t-C_{b1}-C_{a1}$ is smaller than 2°. Meanwhile, the C−C bonds ($C_{b1}-C_{s1}$, $C_{b2}-C_{s2}$, $C_{b1}-C_{a1}$, and $C_{b2}-C_{a2}$) which may involve in hyperconjugation with the forming bond in the transition state differ by 0.007 and 0.008 Å for **1** and **3H**, respectively. The C_s symmetry of the dioxa cages **1** and **3H** is clearly shown with data presented in Table 2. The plane bisecting the angle $C_{b1}-C_t-C_{b2}$ is the C_s symmetry plane.

With the presence of a third oxygen atom (labeled as O_s) in the cage, trioxa cages **2** and **4H** distort slightly

(27) Mehta, G.; Ravikrishna, C.; Ganguly, B.; Chandrasekhar, J. *J. Chem. Soc., Chem. Commun.* **1997**, 75.
(28) (a) Rondan, N. G.; Houk, K. N.; Moss, R. A. *J. Am. Chem. Soc.* **1980**, *102*, 1770. (b) Moss, R. A. *Acc. Chem. Res.* **1989**, *22*, 15. (c) Sakai, S. *Int. J. Quantum Chem.* **1998**, *70*, 291.
(29) (a) Reed, A. E.; Weinhold, F. *J. Chem. Phys.* **1983**, *78*, 4066. (b) Reed, A. E.; Curtiss, L. A.; Weinhold, F. *Chem. Rev.* **1988**, *88*, 889.
(30) Meyers, A. I.; Seefeld, M. A.; Lefker, B. A.; Blake, J. F. *J. Am. Chem. Soc.* **1997**, *119*, 4565.
(31) Wu, Y.-D.; Li, Y.; Na, J.; Houk, K. N. *J. Org. Chem.* **1993**, *58*, 4625.
(32) Gaussian 94, Revision E.2: Frisch, M. J.; Trucks, G. W.; Schlegel, H. B.; Gill, P. M. W.; Johnson, B. G.; Robb, M. A.; Cheeseman, J. R.; Keith, T. A.; Petersson, G. A.; Montgomery, J. A.; Raghavachari, K.; Al-Laham, M. A.; Zakrzewski, V. G.; Ortiz, J. V.; Foresman, J. B.; Cioslowski, J.; Stefanov, B. B.; Nanayakkara, A.; Challacombe, M.; Peng, C. Y.; Ayala, P. Y.; Chen, W.; Wong, M. W.; Andres, J. L.; Replogle, E. S.; Gomperts, R.; Martin, R. L.; Fox, D. J.; Binkley, J. S.; Defrees, D. J.; Baker, J.; Stewart, J. P.; Head-Gordon, M.; Gonzalez, C.; Pople, J. A. Gaussian, Inc., Pittsburgh, PA, 1995.
(33) Gaussian 98, Revision A.5: Frisch, M. J.; Trucks, G. W.; Schlegel, H. B.; Scuseria, G. E.; Robb, M. A.; Cheeseman, J. R.; Zakrzewski, V. G.; Montgomery, J. A., Jr.; Stratmann, R. E.; Burant, J. C.; Dapprich, S.; Millam, J. M.; Daniels, A. D.; Kudin, K. N.; Strain, M. C.; Farkas, O.; Tomasi, J.; Barone, V.; Cossi, M.; Cammi, R.; Mennucci, B.; Pomelli, C.; Adamo, C.; Clifford, S.; Ochterski, J.; Petersson, G. A.; Ayala, P. Y.; Cui, Q.; Morokuma, K.; Malick, D. K.; Rabuck, A. D.; Raghavachari, K.; Foresman, J. B.; Cioslowski, J.; Ortiz, J. V.; Stefanov, B. B.; Liu, G.; Liashenko, A.; Piskorz, P.; Komaromi, I.; Gomperts, R.; Martin, R. L.; Fox, D. J.; Keith, T. A.; Al-Laham, M. A.; Peng, C. Y.; Nanayakkara, A.; Gonzalez, C.; Challacombe, M.; Gill, P. M. W.; Johnson, B. G.; Chen, W.; Wong, M. W.; Andres, J. L.; Head-Gordon, M.; Replogle, E. S.; Pople, J. A. Gaussian, Inc., Pittsburgh, PA, 1998.
(34) Hehre, W. J. et al. SPARTAN, Version 4.1.1, Wavefunction, Inc, 18401 Von Karman Ave., #370, Irvine, CA 92715.
(35) NBO 4.0. Glendening, E. D.; Badenhoop, J. K.; Reed, A. E.; Carpenter, J. E.; Weinhold, F. Theoretical Chemistry Institute, University of Wisconsin, Madison, WI, 1996.

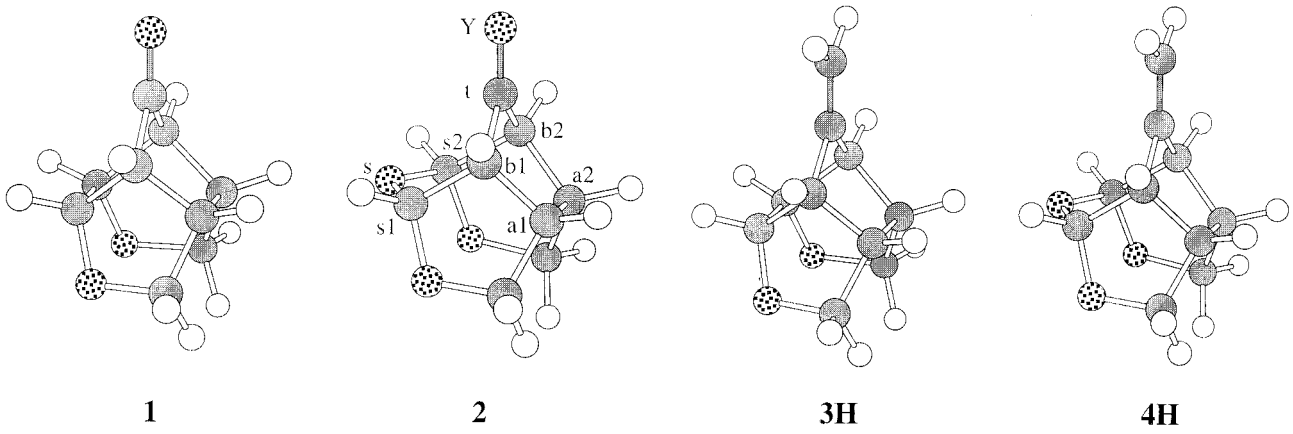

Figure 1. Structures and atom labels of calculated cage compounds. Geometry optimized structures at the theory level of HF/6-31G* are shown. Gray, white, and mosaic circles represent carbon, hydrogen, and oxygen atoms, respectively; (Y) the ketone oxygen or terminal alkene carbon, (t) trigonal carbon, (b) bridgehead, (s) syn, (a) anti, (1) front, and (2) rear positions, respectively. For example, C_{s1} represents the carbon atom located at front position of syn face and H_{s1} is the hydrogen attached to the carbon C_{s1}.

Table 2. Selected Structural Parameters of Substrates Optimized at the HF/6-31G* Level[a]

	1	2	2-sym	3H	4H	4H-sym
dihedral angle[b] (deg)						
$Y-C_t-C_{b1}-H_{b1}$	0.6(*s*)	9.7(*a*)	10.1	0.5(*a*)	8.7(*a*)	9.2
$Y-C_t-C_{b2}-H_{b2}$	0.6(*s*)	10.4(*a*)	10.1	0.5(*a*)	9.8(*a*)	9.2
$Y-C_t-C_{b1}-C_{s1}$	131.0	116.2	115.8	129.3	117.5	116.8
$Y-C_t-C_{b2}-C_{s2}$	131.0	115.3	115.8	129.3	116.1	116.8
$Y-C_t-C_{b1}-C_{a1}$	129.5	136.5	136.8	130.7	134.7	135.2
$Y-C_t-C_{b2}-C_{a2}$	129.5	137.2	136.8	130.7	135.9	135.2
bond length (Å)						
$C_{b1}-C_{s1}$	1.540	1.550	1.549	1.540	1.549	1.547
$C_{b2}-C_{s2}$	1.540	1.548	1.549	1.540	1.545	1.547
$C_{b1}-C_{a1}$	1.547	1.540	1.540	1.548	1.543	1.544
$C_{b2}-C_{a2}$	1.547	1.541	1.540	1.548	1.545	1.544
angle (deg)						
$Y-C_t-O_s$	130.0	130.0	131.7	131.8		
nonbonded distance (Å)						
C_t-O_s	2.588	2.588	2.622	2.621		

[a] **2-sym** and **4H-sym** are the structures of C_s symmetry for **2** and **4H**. [b] Absolute values of dihedral angles are shown in the table; symbols, *s* and *a*, in parentheses indicate the bridgehead hydrogens lean toward syn and anti faces, respectively.

out of the C_s symmetry. Therefore, geometry parameters related to the atoms in the front (e.g., C_{b1}, H_{b1}, C_{s1}) are inequivalent to those in the rear (C_{b2}, H_{b2}, C_{s2}). The bridgehead hydrogens lean toward the anti face by ca. 10° (see dihedral angles $Y-C_t-C_{b1}-H_{b1}$ and $Y-C_t-C_{b2}-H_{b2}$ in Table 2). More importantly, dihedral angles that are related to the accessibility of different faces of the reaction center, $Y-C_t-C_{b1}-C_{s1}$, $Y-C_t-C_{b2}-C_{s2}$, $Y-C_t-C_{b1}-C_{a1}$, and $Y-C_t-C_{b2}-C_{a2}$, show obvious inequivalently of the two faces. According to these angles (Table 2), the anti face of **2** and **4H** is more open than the syn by nearly 20°. Meanwhile, the third oxygen atom, O_s, is 2.6 Å away from the trigonal carbon, C_t, and the $Y-C_t-O_s$ angle is 130°. Therefore, O_s not only cause different accessibility of syn and anti faces (defined by $Y-C_t-C_b-C_s$ and $Y-C_t-C_b-C_a$), it also blocks the bottom part of the syn face. Another change brought by O_s to the atoms next to the reaction center is that C−C bonds which are candidates for hyperconjugation with the incipient bond are slightly longer in the syn face ($C_{b1}-C_{s1}$, $C_{b2}-C_{s2}$) than in the anti face ($C_{b1}-C_{a1}$ and $C_{b2}-C_{a2}$). This is contrary to what are observed in dioxa cages **1** and **3H**. Finally, it is also noted that we have located structures of C_s symmetry for **2** and **4H** (Table 2, **2-sym** and **4H-sym**). These structures have very small imaginary frequency and the energies are virtually identical to that of the "ground state". As can be seen in Table 2, the structural parameters of symmetry and unsymmetrical trioxa cages are similar. All structural features described above for the unsymmetrical structures also apply to the symmetrical ones.

Although the inferior accessibility of the syn face of **2** and **4H** can be used to rationalize the high facial selectivity for anti attack, it is important to have a full understanding of other factors influencing the selectivity. Otherwise, one will not have an integrated view about facial difference of dioxa and trioxa cages **1**−**4**. First, we look at frontier orbitals of these cages. Structural asymmetry of dioxa ketone **1** is minor in the vicinity of the carbonyl group as shown in Table 1, nevertheless, the unequal facial distribution of LUMO coefficient is obvious as shown in Figure 2(a). Comparison of syn and anti faces around reaction center atom C_t shows that there is more significant LUMO coefficient (darker color marked with a "+") found for the syn face. For the more distorted trioxa ketone **2**, there is larger LUMO coefficient found for the anti face, contrary to that of **1**. Other than frontier

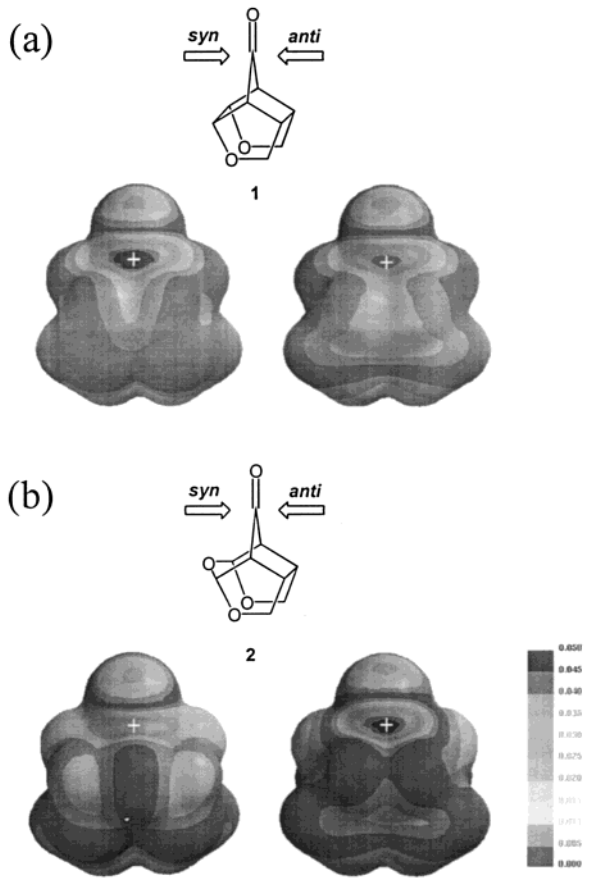

Figure 2. Lowest unoccupied molecular orbital (LUMO) mapped onto the isosurface with an electron density of 0.002 au for **1** (upper-half, (a)) and **2** (lower-half, (b)), respectively. Pictures on the left and right are images viewed from syn and anti faces, respectively. The position of the carbonyl carbon (C_t) is labeled with a plus sign.

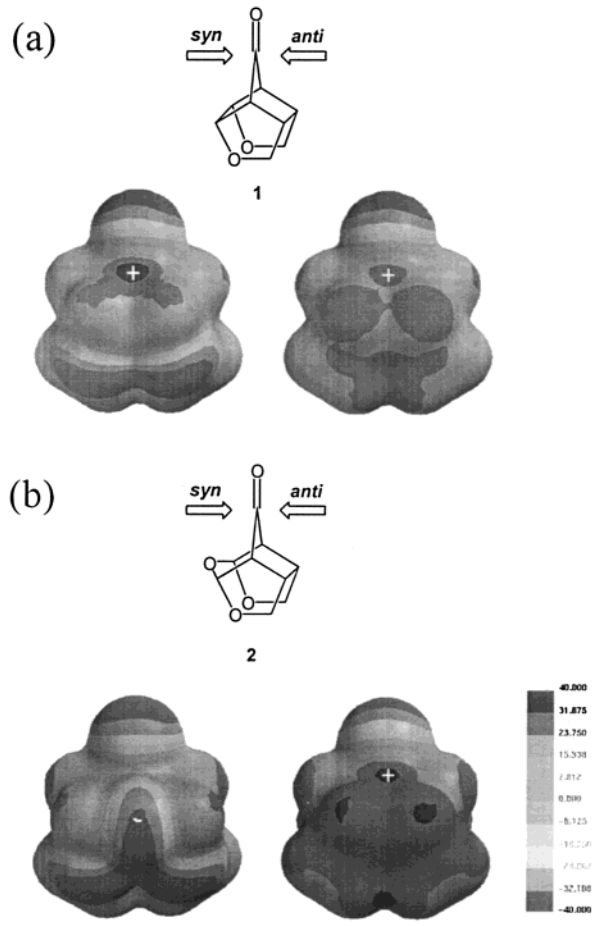

Figure 3. Molecular electrostatic potential (MEP) mapped onto the isosurface with an electron density of 0.002 au for **1** (upper-half, (a)) and **2** (lower-half, (b)). The positions of the most positive and negative values are indicated with plus and minus signs, respectively.

orbitals, molecular electrostatic potentials (MEPs) have also been found useful in predicting reaction sites.[36] For **1**, the more electron deficient nature (darker color marked with a "+") of the syn face than the anti face of the carbonyl carbon atom can be clearly seen in Figure 3a. However, for **2** the syn face MEP above the carbonyl carbon atom is less positive than that of the anti face because of the oxygen atom (O_s) ca. 2.6 Å away. On the basis of LUMO and MEP of the reactant ground state, one would predict the hydride reduction to take place in the syn face for **1** and the anti face for **2**, consistent with experimental findings.

For the ene addition, the unsymmetrical facial distribution of HOMO coefficient of dioxa ene **3H** and trioxa **4H** (Figure S1) is not so obvious as the frontier orbitals (LUMOs) of **1** and **2** (Figure 2), but the facial difference of LUMO coefficient is more prominent (Figure 4). The LUMO coefficient above the inner ene carbon atom has a higher value in the syn face than the anti for **3H** and the reverse is true for **4H**. This leads to the prediction that in trajectory ***a***, where the nonbonded lone pair orbital of the carbon atom of dichlorocarbene is pointing at the empty orbital above the inner ene carbon atom, **3H** should favor syn attack and **4H** favor anti attack. This is in line with the energy trends listed in Table 1 for trajectory ***a***.

Although dichlorocarbene is not so ionic as metal hydrides, the MEPs of dichlorocarbene and ene compounds can be used to rationalize the energy trends of trajectories ***a*** and ***b*** for each facial attack. It is evident from the MEP of dichlorocarbene (Figure S2) that this molecule can be considered as a dipole with its negative end at the nonbonded lone pair electrons of the carbon atom (this direction is confirmed by calculation). The MEPs of **3H** and **4H** (Figure 5) show positive electrostatic potentials on the isodensity surfaces in the area of cage hydrogen atoms H_{s1}, H_{s2}, H_{a1}, and H_{a2} (e.g., see gray and black areas in the middle of **3H** in Figure 5) and negative electrostate potentials in the area of C=C, except for the syn face of **4H**. The presence of O_s makes the MEP of the syn face of **4H** largely negative. Based on an electrostatic argument, one would predict that trajectory ***a*** is preferred over ***b*** for **3H** and for anti attack of **4H**. This is because the negative end of dichlorocarbene is pointing to the positive area of **3H**/**4H**(anti) in trajectory ***a***. For syn attack of trioxa cage **4H** the negative end of dichlorocarbene will be in the vicinity of an oxygen atom (O_s) in trajectory ***a***, so trajectory ***b*** is preferred instead.

(36) (a) *Molecular Electrostatic Potentials: Concepts and Applications*; Murray, J. S., Sen, K., Eds.; Elsevier: Amsterdam, 1996. (b) *Chemical Applications of Atomic and Molecular Electrostatic Potentials: Reactivity, Structure, Scattering, and Energetics of Organic, Inorganic, and Biological Systems*; Politzer, P., Truhlar, D. G., Eds.; Plenum Press: New York, 1981.

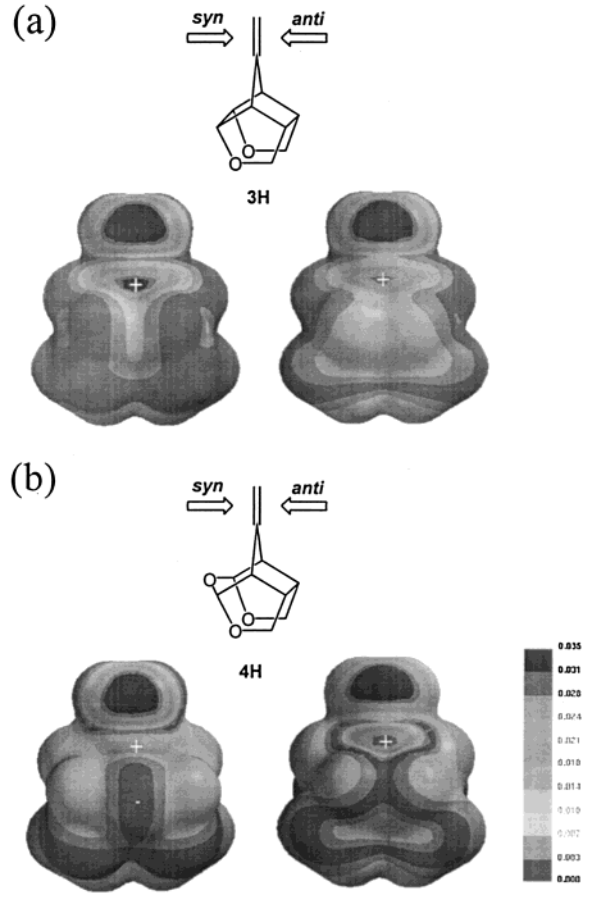

Figure 4. Lowest unoccupied molecular orbital (LUMO) for **3H** (upper-half, (a)) and **4H** (lower-half, (b)), respectively. The position of carbonyl carbon (C_t) is labeled with a plus sign.

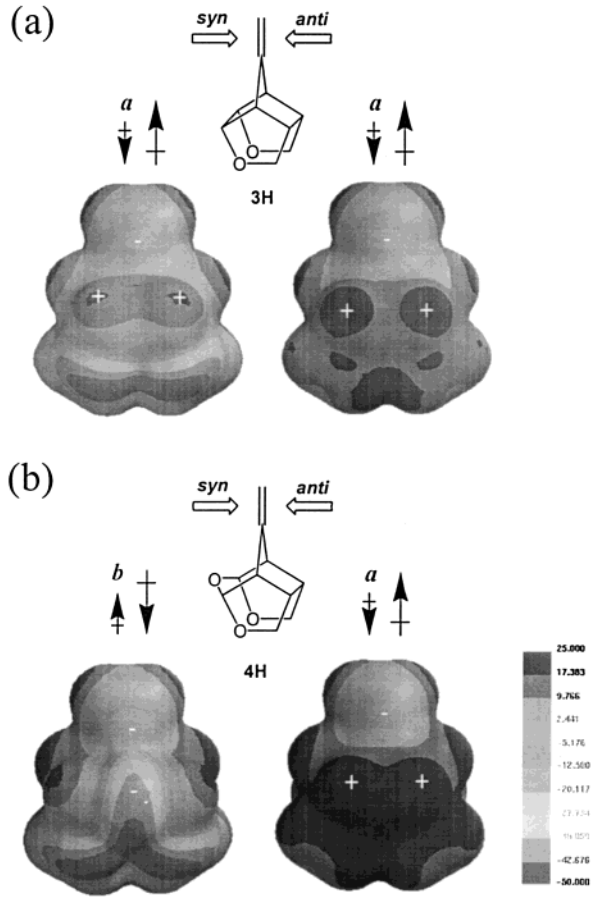

Figure 5. Molecular electrostatic potential (MEP) for **3H** (upper-half, (a)) and **4H** (lower-half, (b)). The positions of the most positive and negative values are indicated with plus and minus signs, respectively. The preferred directions of the dipole moment of dichlorocarbene (small arrows) are labeled for each facial attack (large arrows are for the local dipole direction in the vicinity of reaction centers of **3H** and **4H**). Labels ***a*** and ***b*** represent the addition trajectories with the carbon lone pair of dichlorocarbene pointing to the inner ene carbon, C_t, and the outer one, Y, respectively.

The above deduction complies with the switch in attacking trajectory described in the previous section and in Table 1.

Transition Structure. For the nearly structurally unbiased dioxa cages **1** and **3H**, the transition structures of syn and anti attacks are very similar (Figures 6 and 7). For trioxa ketone **2**, the C═O and forming H^--C bonds in the anti transition structure (1.236 and 1.978 Å) are longer and shorter than the counterparts in the syn transition structure (1.229 and 2.161 Å), respectively. Therefore, the transition structure of the anti attack is later than that of the syn attack. One interesting phenomenon of transition structures of hydride reduction of **2** is that **2-*anti*** is symmetrical, whereas **2-*syn*** is unsymmetrical. As mentioned previously, the potential energy difference between symmetrical and unsymmetrical **2** is negligible. Therefore, it is easy for **2** to adopt a structure that is most suitable for hydride attack. For the anti attack, because the number and types of atoms the hydride feels along the reaction path are the same in the front part (C_{b1}, C_{a1}, H_{b1}, H_{a1}) and in the rear (C_{b2}, C_{a2}, H_{b2}, H_{a2}), it is not surprising that **2-*anti*** is of C_s symmetry. For the syn attack, the H^--C−O attacking angle (95°) is smaller than that of **2-*anti***, **1-*syn*** and **1-*anti*** (98−99°). The distance between H^- and O_s (2.768 Å) is not much longer than the sum of VDW radii of neutral H and O, 2.6 Å. Furthermore, O_s deviates from H_{s1}−C_{s1}−C_{s2} (or H_{s2}−C_{s2}−C_{s1}) plane in the syn transition structure by ca. 40°, which is 20° larger than that in the ground state. The C_t···O_s distance, 2.774 Å, is also longer than that of the ground state (2.588 Å). These structural features of **2-*syn*** imply that the incoming hydride has experienced strong influence of O_s and the two atoms are trying to avoid each other. The inferior accessibility of the syn face has been overcome by downward movement of O_s and deformation of the Li−H...C═O transition structure. We believe that the trioxa cage distorts out of the C_s symmetry to minimize the repulsion between O_s and hydride. For example, the H^-···O_s distance can be lengthened if the cage is distorted.

In Figure 6, all the C−C bonds antiperiplanar to the forming bond are longer than that of the corresponding bond in the ground-state reactant, as what would be predicted on the basis of a hyperconjugative model. For example, in **1-*syn***, the antiperiplanar C_{b1}−C_{a1} and C_{b2}−C_{a2} bonds (1.553 Å) are 0.006 Å longer than that of the ground-state reactant (1.547 Å in Table 2). On the other hand, the periplanar C−C bonds (such as C_{b1}−C_{s1} in **1-*syn***) of all hydride reduction transition structures are shorter in the transition state than in the ground state. Taking **1-*syn*** again as an example, the C_{b1}−C_{s1} bond is 1.534 Å in the transition structure and 1.540 Å in the ground state. The shortening of periplanar bonds can be rationalized by hyperconjugation model as well. When

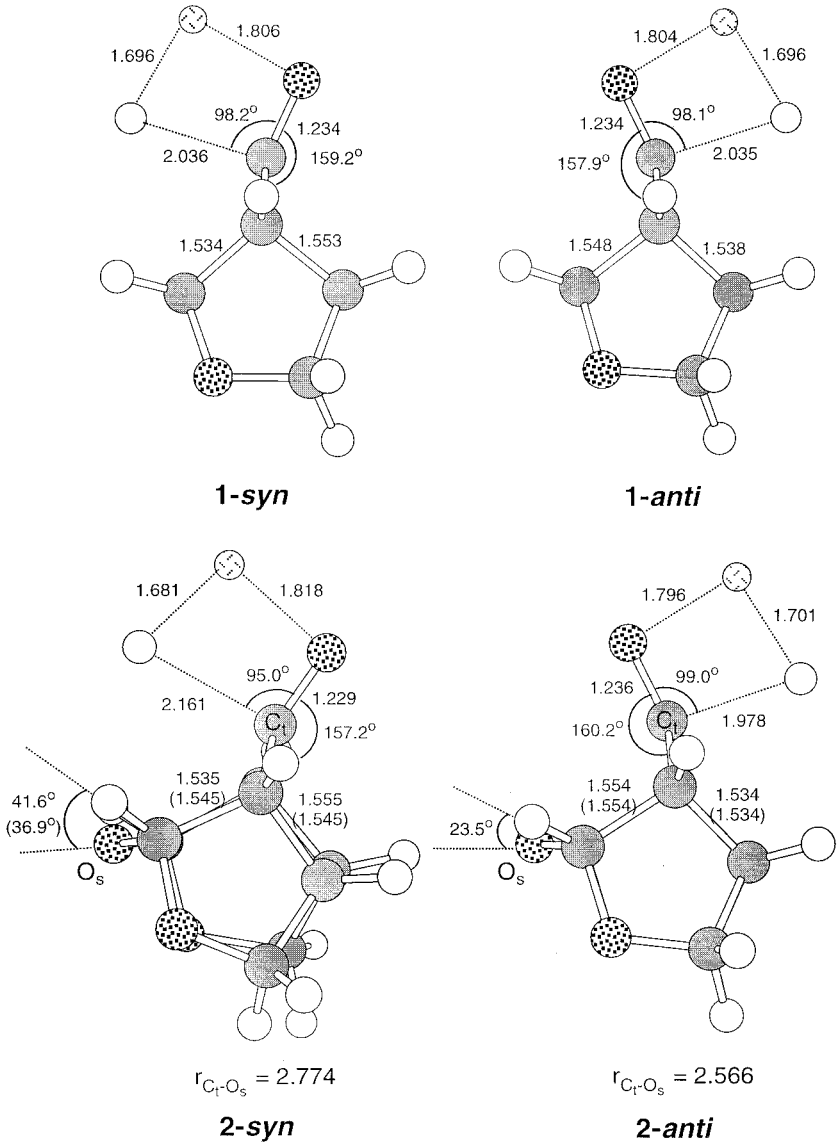

Figure 6. Transition structures of LiH addition to substrates, **1** (upper-half) and **2** (lower-half) at the theory level of HF/6-31G*. Selected geometric parameters are shown with distance in unit of Å and angle in unit of degree. Geometric parameter of the rear part is shown in parentheses or not shown when it is the same as the front one. Labels of syn and anti represent the addition from syn and anti faces with respect to the oxygen atoms of heterorings, respectively.

the hydride attacks the carbonyl C═O antibonding orbital, the carbonyl group C═O bents away from the face of addition, as shown in Figure 6. In this addition process, the C═O antibonding orbital develops into the H⁻−C forming bond and overlaps less and less with the periplanar C−C bonds due to the bending motion of C═O. With loss of hyperconjugation with an empty orbital, the periplanar C−C bonds become shorter.

For dichlorocarbene addition, characteristics of transition structures of trajectories ***a*** (in which carbene forms partial bonding with the inner alkene atom to a greater extent) and ***b*** (carbene forms partial bonding with the terminal carbon atom to a greater extent) are very different (Figures 7 and 8). For trajectory ***a***, distances of the two newly forming bonds differ by less than 0.18 Å in both syn and anti attacks of **3H** and **4H** (**3H$_a$-*syn***, **3H$_a$-*anti***, **4H$_a$-*syn***, and **4H$_a$-*anti***). The attacking angles (formed by the major forming bond and the double bond) are ca. 79° and the tilt angles of carbene from the line parallel to the alkene double bond are ca. 35°. It is noted that in the presence of an additional oxygen atom in the trioxa cage, the geometry of reaction center in **4H$_a$-*syn*** does not differ significantly from that of **3H$_a$-*syn***, **3H$_a$-*anti***, and **4H$_a$-*anit***, unlike the change of attacking angles in **2-*syn*** (Figure 6). Nevertheless, O_s still moves downward in **4H$_a$-*syn*** as in **2-*syn***. This implies that 1) the repulsion between O_s and $:CCl_2$ is smaller than between O_s and H^- and 2) movement of O_s is relatively easy.

For trajectory ***b***, the distance differences, attacking angles and tilt angles of **3H$_b$-*syn***, **3H$_b$-*anti***, and **4H$_b$-*anti*** are ca. 0.57 Å, 98°, and 47°, respectively. These values are significantly larger than those in trajectory ***a***. The geometry around the reaction center of **4H$_b$-*syn*** differs from the other three transition structures of trajectory ***b*** in that its forming bonds are slightly shorter (ca. 0.02 Å) and the tilt angle is larger by 3°. It is noted that a large distance difference between the two forming bonds has been reported for alkene with steric hindrance around one of the alkene carbon atom.[37] Examination of the Cl···H_s and Cl···H_a distances shows that they are all around 3.0 Å (Figures 7 and 8), equal to the sum of VDW

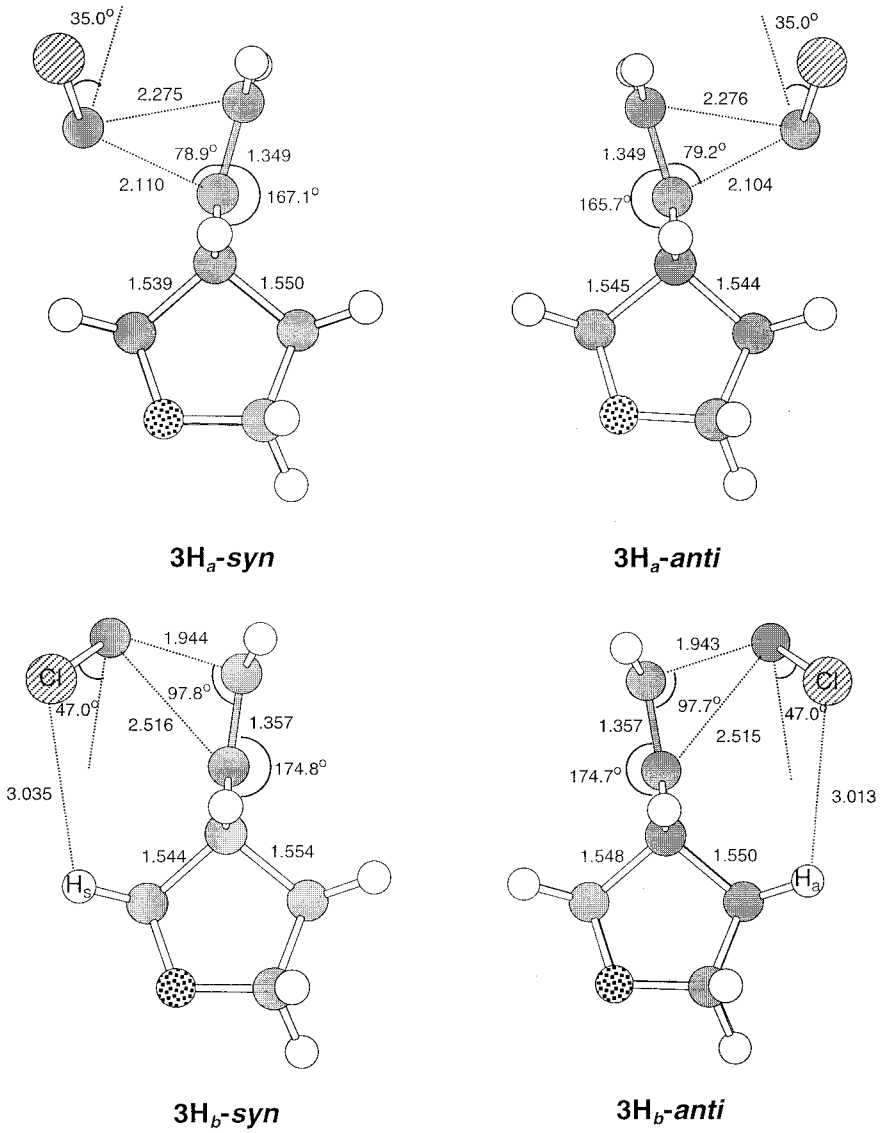

Figure 7. Transition structures of dichlorocarbene addition to **3H** at the theory level of HF/6-31G*.

radii of Cl and H atoms. These short Cl···H distances and the long $C_{carbene}$···C_t distances (ca. 2.5 Å) imply steric requirement is playing a role in large difference of forming bonds, attacking angle and tilting angle in trajectory ***b***.

Torsional Strain Effect. Analysis of the torsion angles around the Newman projections with a view down to the $C_{b1}-C_t$ and $C_{b2}-C_t$ bonds can provide information related to the torsion strain effect. It can further afford as a criterion to judge which structure (syn or anti) is more favored. In general, a favored transition structure should prefer a good alignment between the forming bond and antiperiplanar bond, prefer a staggered attacking angle, and minimize the structural change from reactant to transition structure. This is because a good alignment gains more stabilization energy from hyperconjugation interaction, a staggered attacking angle minimizes the bond-bond repulsion, and minimal structure distortion requires less energy to deform the reactant.

The torsion angles around $C_{b1}-C_t$ and $C_{b2}-C_t$ bonds are listed in Table 3. Trajectory ***b*** of carbene addition is not listed because in this trajectory dichlorocarbene basically attacks the terminal carbon atom. Therefore, torsional strain in trajectory ***b*** should not be as important as in all other transition structures where the reaction center is part of a ring. According to Table 3, the alignment between the forming bond and antiperiplanar bond can be judged by the sum of torsion angles 1, 5, and 6. As the ground state **1** and **3H** are rather symmetrical, the difference in alignment between transition structure of dioxa cages is minor. For trioxa cages, better alignment ($1 + 5 + 6 \approx 180°$) between the forming and antiperiplanar bonds is observed in **2-*anti*** (168.3°) than in **2-*syn*** (150.6°, 155.2°). A similar observation is made for trajectory ***a*** of **4H** (**4H$_a$-*anti***: 176.6°; **4H$_a$-*syn***: 163.5°, 159.3°). Therefore, in our system the transition structure of the experimentally favored attacking face does provide better alignment for hyperconjugation.

Examination of angles 1 and 2 shows the attacking angles of **2-*anti*** (60.7 for angle 1 and 67.8° for angle 2) and **4H$_a$-*anti*** (68.8° and 58.8°) are more staggered than that of **2-*syn*** (averaged 46.0° for angle 1 and 84.0° for angle 2) and **4H$_a$-*syn*** (averaged 53.9° and 74.8°), respectively. As for distortion around the reaction center in the

(37) Bernardi, F.; Bottoni, A.; Canepa, C.; Olivucci, M.; Robb, M. A.; Tonachini, G. *J. Org. Chem.* **1997**, *62*, 2018.

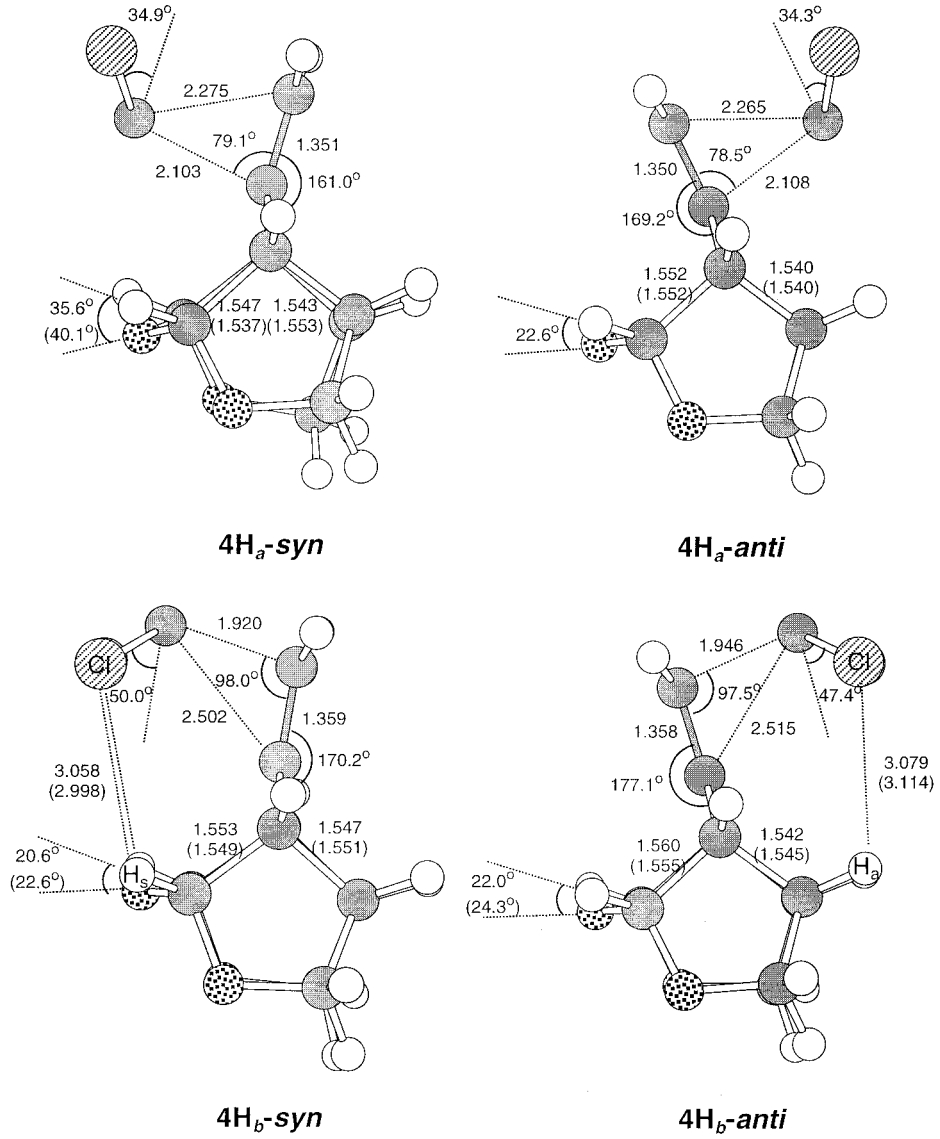

Figure 8. Transition structures of dichlorocarbene addition to **4H** at the theory level of HF/6-31G*.

transition structure relative to the ground state, we choose torsion angle 3 to represent the movement of C═O and C═C upon addition reactions, sum of angles 1 and 2 to reflect the impact of the attacking reagent to atoms close to it, and angles 5 and 6 to detect the distortion of cage rings. The angle difference (Δ) between the transition structure and ground state is listed in Table 3. It is found that the difference of different facial attacks of dioxa cage is in general small, but the difference of trioxa cage is more significant. The angle differences Δ of **2-*anti*** for angles 3, 1 + 2, 5, and 6 are ca. 28°, 2°, 3°, and 3°, respectively. All are smaller than the corresponding values of **2-*syn*** (ca. 30°, 4°, 8°, and 8°, respectively). The same trend is observed for **4H$_a$-*anti*** and **4H$_a$-*syn***. This reflects that the trioxa cage suffers less structural distortion upon anti addition.

Although it is mentioned that geometries in the vicinity of the reaction center are rather similar in syn and anti transition structures for dioxa cages **1** and **3H**, the strain experienced by the substrate may contribute differently to activation energies of the syn and anti attacks. The distorted energy E_{sub} listed in Table 4 shows the energy differences of cage compounds frozen in their transition structure without the inclusion of attacking reagent. It is found for **1** and **3H** that the distorted energy of the syn attack is lower than that in the anti attack. On the other hand, for **2** and **4H**, the E_{sub} in the anti attack is lower. These trends echo the product ratios observed experimentally and structural analysis presented above. Therefore, not only the syn faces of **1** and **3H** and anti faces of **2** and **4H** are more reactive than their counterparts based on the frontier orbital or MEP analyses, the skeletons of the cage compounds are also more apt to adopt distortion in the transition structures of the more reactive faces.

Electrostatic and Hyperconjugative Interactions. In Table 4 we list the energy differences between syn and anti faces from calculations in which the attacking reagents in the transition structure are replaced with point charges obtained from natural population analysis. In Charge Model I, all the atoms of the attacking reagent are replaced with charges. In Charge Model II, we followed Mehta,[25a,27] Houk,[10] and others to use the "charge replacement model" only for the hydride, but not for the metal ion. Mehta has also used hydride to illustrate the combined effect of electrostatic and hyper-

Table 3. Torsion Angles of Transition Structures around the C_b-C_t Bond[a]

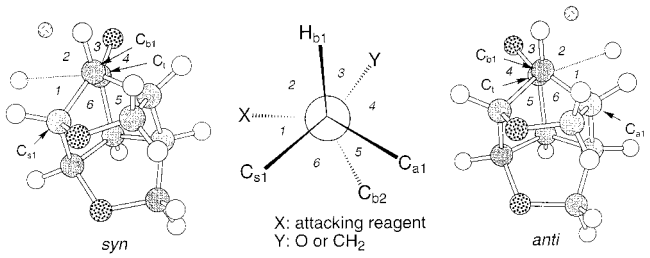

	transition														
	1	2	1 + 2			3			5			6			1 + 5 + 6
structure[b]	TS	TS	TS	G	Δ	TS	G	Δ	TS	G	Δ	TS	G	Δ	TS
1-*syn*	54.4	78.6	133.0	130.4	2.6	28.3	0.6	27.7	54.5	50.1	4.4	45.3	49.4	4.1	154.2
	54.4	78.6	133.0	130.4	2.6	28.3	0.6	27.7	54.5	50.1	4.4	45.3	49.4	4.1	154.2
1-*anti*	55.7	77.6	133.3	130.1	3.2	29.9	−0.6	30.5	54.6	49.4	5.2	45.0	50.1	5.1	155.3
	55.7	77.6	133.3	130.1	3.2	29.9	−0.6	30.5	54.6	49.4	5.2	45.0	50.1	5.1	155.3
2-*syn*	43.2	85.9	129.1	126.0	3.1	18.2	−9.7	27.9	46.5	41.4	5.1	60.9	65.9	5.0	150.6
	48.7	82.1	130.8	125.7	5.1	21.9	−10.4	32.3	51.1	40.6	10.5	55.4	66.9	11.5	155.2
2-*anti*	60.7	67.8	128.5	126.7	1.8	38.5	9.7	28.8	69.8	65.9	3.9	37.8	41.4	3.6	168.3
	60.7	67.8	128.5	126.8	1.7	38.5	10.4	28.1	69.8	66.9	2.9	37.8	40.6	2.8	168.3
3H$_a$-*syn*	61.6	70.1	131.7	129.8	1.9	18.1	−0.5	18.6	53.1	49.7	3.4	47.0	50.3	3.3	161.7
	61.6	70.1	131.7	129.8	1.9	18.1	−0.5	18.6	53.1	49.7	3.4	47.0	50.3	3.3	161.7
3H$_a$-*anti*	63.0	69.1	132.1	130.2	1.9	20.0	0.5	19.5	53.4	50.3	3.1	46.5	49.7	3.2	162.9
	63.0	69.1	132.1	130.2	1.9	20.0	0.5	19.5	53.4	50.3	3.1	46.5	49.7	3.2	162.9
4H$_a$-*syn*	56.4	73.0	129.4	126.2	3.2	16.7	−8.7	25.4	49.5	42.6	6.9	57.6	65.1	7.5	163.5
	51.4	76.5	127.9	125.8	2.1	13.1	−9.8	22.9	45.1	41.5	3.6	62.8	66.6	3.8	159.3
4H$_a$-*anti*	68.8	58.8	127.6	126.0	1.6	27.2	8.7	18.5	68.8	65.1	3.7	39.0	42.6	3.6	176.6
	68.8	58.8	127.6	126.1	1.5	27.2	9.8	17.4	68.8	66.6	2.2	39.0	41.5	2.5	176.6

[a] Pictures show the definition of the torsion angles. The dotted line connects the attacking atom and the reaction center (carbon C_t). Two sets of torsion angles are shown for each transition structure; the first one and the second one are viewed down to the $C_{b1}-C_t$ and $C_{b2}-C_t$ bonds, respectively. [b] TS, G, and Δ represent the transition structure, ground-state substrate, and the difference between ground-state substrate and transition structure, respectively.

Table 4. Calculated Relative Energies of Substrates in Transition States and the Relative Energies Evaluated with the Charge Model and the Hydride Model[a]

	E_{sub}[b]	charge model I[c]	charge model II[d]	hydride model[e]
1-*syn*	0.00	0.00	0.00	0.00
1-*anti*	0.82	2.89	1.52	1.91
2-*syn*	1.07	5.85	8.18	11.41
2-*anti*	0.00	0.00	0.00	0.00
3H$_a$-*syn*	0.00	0.00		
3H$_a$-*anti*	0.11	0.28		
4H$_b$-*syn*	2.73	4.28		
4H$_a$-*anti*	0.00	0.00		

[a] Optimized Structures at the theory level of HF/6-31G* are used; energy is in units of kcal/mol. [b] Single-point energy of the substrate in the transition structure. [c] Single-point energy of transition structure with the atoms of LiH and $:CCl_2$ replaced by natural population charges. [d] Single-point energy of substrate and hydride in transition structure with hydride replaced by a negative charge of −0.5e. [e] Single-point energy of substrate and hydride in transition structure.

conjugative interactions.[27] This is the Hydride Model in Table 4. We do not think electrostatic or hyperconjugation effects in the transition states can be quantified by any of the above model because a *hard* point charge is quite different from a relatively *soft* attacking reagent. Nevertheless, it should show the trend of facial difference of cage compounds under the influence of these two factors. Results in Table 4 clearly show that electrostatic or the combination of electrostatic and hyperconjugation effects help to achieve the experimentally observed facial differences.

Hyperconjugation of Cieplak and Anh types are based on the concept of donor−acceptor interactions of localized orbitals (lone pairs or bonds). The NBO analysis[29,35] is based on optimally transforming a given wave function into localized forms, which correspond to the one-center ("lone pair") and two-center ("bond") elements in the Lewis structure picture. Donor−acceptor interactions related to hyperconjugation can be estimated by the second-order perturbation analysis implemented in the NBO 4.0 program.[35] In Cieplak and Anh models, the focus is on the hyperconjugation between the orbitals of the forming bond and the vicinal bond, so only the Lewis resonance structures that have a forming bond are chosen for the NBO analysis. The NRT[35,38] module of the NBO 4.0 program determines resonance structures and weights on the basis of molecular electron density. Results of the NRT analysis shows that only one Lewis structure of each transition state bears the forming bond and the weights of these structures are 12.03%, 11.97%, 9.62%, and 25.40% for **1**-***syn***, **1**-***anti***, **2**-***syn***, and **2**-***anti***, respectively. The weight variance can be understood by inspection of geometry of the forming H^--C bond in the transition structure. The weights of **1**-***syn*** and **1**-***anti*** are similar, which agree with the fact that transition structures **1**-***syn*** and **1**-***anti*** bear almost the same attacking angles and forming bond lengths (see Figure 6). For trioxa **2**, the transition structure of **2**-***syn*** is earlier than **2**-***anti*** as mentioned in the transition structure section. Therefore, the weight of bond-forming Lewis structure of **2**-***syn*** is smaller than that of **2**-***anti***.

The donor−acceptor orbital interactions related to the forming bond are collected in Table 5. It is noted

(38) (a) Gladening, E. D.; Weinhold, F. J. *Comput. Chem.* **1998**, *19*, 539. (b) Glendening, E. D.; Weinhold, F. *J. Comput. Chem.* **1998**, *19*, 610. (c) Glendening, E. D.; Badenhoop, J. K.; Weinhold, F. *J. Comput. Chem.* **1998**, *19*, 628.

Table 5. Percentage of Different Types of Hyperconjugative Stabilization Energies with Respect to the Cieplak-Type Hyperconjugation

	anh (%)	O_s (%)
1-*syn*	23.9	
1-*anti*	23.3	
2-*syn*	16.9	
2-*anti*	43.7	12.4
3H$_a$-*syn*	21.2	
3H$_a$-*anti*	20.5	
4H$_b$-*syn*	15.5	
4H$_a$-*anti*	35.1	15.0

that the Lewis resonance structure that bears the idea of a fully formed bond cannot completely represent the transition structure which in fact has a partially formed bond. As a result, the hyperconjugative stabilization energies of the forming bond (Table S1) are overestimated. Moreover, since the resonance weights of syn and anti bond-forming Lewis structure are different, the degrees of overestimation are also different. This difference in degrees of overestimation makes comparison of NBO hyperconjugative stabilization energies between syn and anti transition structures inappropriate. Therefore, we only consider the relative importance of different types of orbital interactions within a transition structure. Within the framework of NBO the Cieplak effect is the major effect (Table S1), so it is taken as 100% to obtain the relative percentage of other hyperconjugations related to the forming bond. For **1**-***syn*** and **1**-***anti***, the magnitudes of the Anh effect are 23.9% and 23.3% of the Cieplak effect, respectively (Table 5). This indicates that no matter how the Cieplak effect favors the syn or anti addition, the Anh effect will give the same facial preference with a magnitude of 23% of the Cieplak effect. In other words, the Cieplak and Anh effects contribute to the facial preference in a cooperative manner. The same argument is true for **3H**. Here, the magnitudes of the Anh effect are 21.1% and 20.5% of the Cieplak effect for syn and anti attacks, respectively. The above results imply that if the transition structures are similar for syn and anti attacks and the magnitude of the Anh effect is a fixed fraction of the Cieplak effect, one can make correct prediction of facial preference by solely examining the Cieplak-type (or Anh-type) interaction.

For trioxa **2**, the lone pair of O_s gives a noticeable contribution to the hyperconjugation with the antibonding orbital of the forming bond in the anti attack, but smaller than Cieplak and Anh effects (Table 5). The magnitudes of the Anh effects are 16.9% and 43.7% of the Cieplak effects for syn and anti attacks, respectively. In other words, the Anh effect weights more in the anti than in the syn addition. It implies that if the Cieplak effect favors the anti attack, the Anh effect will also give the same facial preference. On the other hand, if the Cieplak effect favors syn and anti additions to the same extent or favors syn addition slightly more, the combination of Anh effect and O_s contribution may have the chance to override the Cieplak effect to favor the anti addition. The same reasoning applies to trioxa **4H**. It clearly demonstrates that if the transition structures are not similar, judging the attacking preference solely by the Cieplak effect (or Anh effect) may lead to a wrong prediction.

Conclusion

We have carried out ab initio calculations of addition reactions of dioxa and trioxa cage compounds **1**, **2**, **3H**, and **4H**. The calculated relative energies of transition structures reproduce the trend of facial selectivity observed in experiment. We then looked at facial selectivity from the points of view of structure, frontier orbitals and MEP of the reactants, as well as strain, electrostatic, and hyperconjugation effects in the transition state.

For dioxa cages **1** and **3H**, the structural facial difference around the reaction center is minor. Nevertheless, the electronic difference of syn and anti faces generated by the two remote oxygen atoms is clearly demonstrated via frontier orbital and MEP analyses. For trioxa cages **2** and **4H**, the close proximity of the third ether oxygen (O_s) to the reaction center brings large structural and electronic changes around the reaction center. The syn face, which is more reactive in dioxa cages, is less accessible and less reactive than the anti face in trioxa cages.

Analyses based on transition structures reveal several common features of our cage compounds. First of all, electrostatic interactions approximated by the charge replacement calculations afford facial difference in line with the transition state energies. Secondly, the more reactive faces are more apt to adopt structural distortion in the transition state. Moreover, the calculated electrostatic and strain energy differences of syn and anti transition structures are significantly larger for trioxa cages than for the dioxa cages. Therefore, they both contribute to the enhanced facial selectivity of trioxa compounds. Finally, analysis of hyperconjugative stabilization in the transition state reveals the danger of relying solely on Cieplak or Anh models in rationalization of facial selectivity, especially when non-equivalent steric and electrostatic effects as those present in the trioxa systems are involved.

Acknowledgment. This work was supported by the National Science Council and Academia Sinica, Taiwan (ROC). The granting of computing time from the National Center for High-performance Computing and Computing Center of Academia Sinica is acknowledged. The helpful comments from the reviewers are also acknowedged.

Supporting Information Available: HOMO of **3H** and **4H** (Figure S1) and MEP of :CCl_2 (Figure S2). Hyperconjugative stabilization energies estimated by NBO second-order perturbation analysis (Table S1). This material is available free of charge via the Internet at http://pubs.acs.org.

JO000872J